pubs.acs.org/Biomac

Article

Natural and Engineered Isoforms of the Inflammasome Adaptor ASC Form Noncovalent, pH-Responsive Hydrogels

Eduardo A. Gaspar-Morales, Anthony Waterston, Mourad Sadqi, Pedro Diaz-Parga, Ariell M. Smith, Arvind Gopinath, Roberto C. Andresen Eguiluz, and Eva de Alba*

Cite This: *Biomacromolecules* 2023, 24, 5563−5577

Read Online

ACCESS | Metrics & More | Article Recommendations | Supporting Information

ABSTRACT: The protein ASC polymerizes into intricate filament networks to assemble the inflammasome, a filamentous multiprotein complex that triggers the inflammatory response. ASC carries two Death Domains integrally involved in protein self-association for filament assembly. We have leveraged this behavior to create noncovalent, pH-responsive hydrogels of full-length, folded ASC by carefully controlling the pH as a critical factor in the polymerization process. We show that natural variants of ASC (ASC isoforms) involved in inflammasome regulation also undergo hydrogelation. To further demonstrate this general capability, we engineered proteins inspired by the ASC structure that also form hydrogels. We analyzed the structural network of the natural and engineered protein hydrogels using transmission and scanning electron microscopy and studied their viscoelastic behavior using shear rheology. Our results reveal one of the very few examples of hydrogels created by the self-assembly of globular proteins and domains in their native conformation and show that Death Domains can be used alone or as building blocks to engineer bioinspired hydrogels.

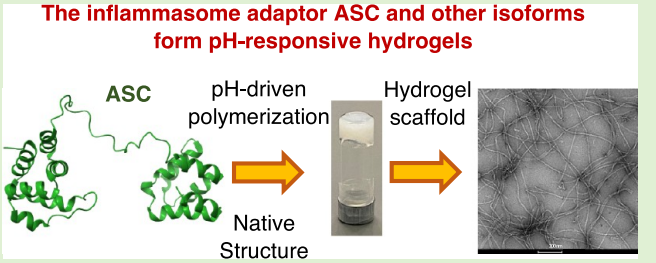

INTRODUCTION

Protein- and peptide-based hydrogels are desirable biomaterials for biomedical applications because of their inherent biodegradability, the potential to incorporate a vast variety of functions, and their capability to respond to stimuli.[1−6] Biomedical applications of biological hydrogels include emulating artificial extracellular matrices as scaffolds for tissue engineering, drug delivery by controlled release, biomaterials for wound repair and surgery procedures, biosensors, and imaging.[6−8] In addition, reconstituted protein-based hydrogels are used to study the function and properties of biological hydrogels such as mucus.[9] Thus, intensive research and bioengineering efforts are currently being directed to design and produce new protein-based hydrogels with tunable mechanical properties and specific functionalities.

Most currently known protein-based hydrogels are composed of fibrous proteins, such as collagen, and proteins that are major components of the extracellular matrix, like elastin.[3,10−12] In contrast, globular proteins in their native state are far less commonly capable of transitioning to a hydrogel state. However, upon denaturation by acidic pH, high temperature, or addition of alcohols, globular proteins unfold acquiring self-assembly capabilities that facilitate hydrogel formation.[5] In addition, numerous examples have been reported of hydrogels formed by the self-assembly of α-helical peptides into coiled coils[1,13−15] and β-sheet forming peptides.[1,5,16] More recently, a few examples have emerged of hydrogels formed by chemical cross-linkage of globular protein domains using enzyme-catalyzed coupling, photo-induced cross-linking, and click-chemistries.[1] Additionally, globular proteins have been used to create hydrogels with physical nonproteinaceous[1,17,18] and proteinaceous[1,19−21] cross-linkages. An elegant example of such hydrogel is based on the high binding affinity between WW domains and polyproline-rich motifs.[22] The design of this all-proteinaceous hydrogel consists of mixing two polypeptides carrying several WW domains and polyproline-rich motifs, spaced by short peptide linkers.

The viscoelastic behavior, specifically the storage or shear modulus, of the different protein-based hydrogels depends on the molecular composition and type of cross-linkage. Importantly, it has been demonstrated that the stability of the globular fold strongly influences the hydrogel's mechanical response.[17,23−25] Thus, globular protein hydrogels may offer a broader scope of applications by increasing elasticity and toughness via the manipulation of the unfolding/folding processes of the globular domains that act as the hydrogel

Received: April 21, 2023
Revised: October 6, 2023
Accepted: October 9, 2023
Published: November 6, 2023

building blocks.[17,23−25] For instance, protein unfolding will result in the extension of the polymer length that could in turn lead to modifications of the viscoelastic behavior.[25]

Notably, few examples of hydrogels formed solely based on the self-assembly of folded proteins have been reported. For example, the folded C-terminal domain of major ampullate spidroin (MaSp1) forms reversible hydrogels at a low temperature (2 °C), whereas a high temperature (65 °C) promotes the protein's partial unfolding leading to irreversible hydrogel formation.[26] Moreover, the fusion of elastin-like polypeptides to this domain has been used to tune the hydrogel temperature response, narrowing it down to more physiological values with applications in cell storage and delivery.[27] In addition, recombinant miniature spidroins, bearing the C- and N-termini or the N-terminus alone, form hydrogels at 37 °C. The hydrogelation process involves a structural conversion into β-sheets for the formation of fibrils.[28]

Here we show that globular Death Domains[29] have the capability to form hydrogels without requiring any molecular helper such as peptide-based or synthetic cross-linkers. To demonstrate hydrogelation and study the properties of hydrogels formed by Death Domains, we used two natural proteins involved in the inflammatory response. Specifically, we have studied hydrogel formation by the natural protein ASC[30−32] and its isoform ASCc,[33] which activate and inhibit the inflammatory response, respectively.[33] The three-dimensional structure of ASC reveals that the protein is composed of two Death Domains, PYD (pyrin) and CARD (caspase activation and recruitment domain), connected by a linker.[31] No structural information is known about ASCc; however, its amino acid sequence suggests an intact CARD connected to an incomplete PYD. In addition, we demonstrate that this behavior is not limited to natural Death Domain proteins, as we have engineered constructs based on the ASC structure to successfully form hydrogels. Finally, we show that these hydrogels are pH-responsive.

MATERIALS AND METHODS

Protein Expression and Purification. Plasmids (pET-15b) encoding the sequences of human ASC, ASCc, and engineered CARD, and CARD−CARD (Supporting Figure S1) were transformed in BL21(DE3) *Escherichia coli* cells. Bacteria were grown overnight in LB medium at 37 °C. Cell cultures were diluted to reach an OD of 0.8 at 600 nm and were subsequently induced for 4 h by the addition of 1 mM IPTG to produce overexpression of the recombinant proteins. The cells were harvested by centrifugation at 8,000 rpm for 30 min at 4 °C. The pellets were resuspended in 20 mM Tris-HCl (pH 8), 500 mM NaCl, 5 mM imidazole, and 6 M guanidine hydrochloride (resuspension buffer) and then sonicated (12 times in 15 s intervals, alternated with 45 s resting periods). The lysed cells were ultracentrifuged at 35,000 rpm for 30 min at 4 °C. The resulting supernatant was filtered to remove cell debris with a 0.45 μm pore size filter. All proteins have a 6-histidine tag at the N-terminus and were purified by nickel affinity chromatography. The chromatographic matrix was equilibrated with the resuspension buffer. After protein binding, the matrix was washed with a buffer containing 20 mM Tris-HCl (pH 8), 500 mM NaCl, 20 mM imidazole, and 6 M guanidine hydrochloride. The purified proteins were eluted in a 45 min gradient with a buffer containing 20 mM Tris-HCl (pH 8), 500 mM NaCl, 500 mM imidazole, and 6 M guanidine hydrochloride. The solutions of the eluted proteins were dialyzed against 1 L of a dialysis buffer containing 0.5 mM TCEP at pH 3.8 using dialysis cassettes, and the buffer was changed 3 times every 2−3 h. The protein solutions were extracted from the dialysis cassette and filtered. All proteins were further purified by reversed-phase chromatography in a C4 column. The C4 matrix was equilibrated with a buffer containing 94.9% H_2O, 5% acetonitrile, and 0.1% trifluoroacetic acid, and the proteins were eluted in a 30−40 min gradient with an elution buffer containing 94.9% acetonitrile, 5% H_2O, 0.1% trifluoroacetic acid. All eluted protein solutions were lyophilized for the removal of organic solvents and stored in a desiccator. All buffers were filtered through 0.2 μm pore size filters.

Peptide Synthesis for the Formation of the CARD-Peptide Hydrogel. The sequence of the peptide from the N- to C-termini is MGRARDAILDALENLTAEELKKFKLQAAT, which encompasses the incomplete PYD domain of ASCc (Supporting Figure S1). This peptide, with no modifications at the N- or C-terminus, was synthesized by solid-phase peptide synthesis by Thermo Fisher with a purity >95%.

Mass Spectrometry. The purity and integrity of the recombinant proteins were determined by mass spectrometry and sodium dodecyl sulfate polyacrylamide gel electrophoresis (SDS-PAGE). For mass spectrometry, the lyophilized protein material was dissolved in a solution containing 95% acetonitrile, 4.9% water, and 0.1% formic acid and injected into an electrospray ionization mass spectrometer (Q-Exactive Hybrid Quadrupole-Orbitrap, Thermo). The molecular weight obtained by mass spectrometry matched the expected molecular weight based on the amino acid sequence for all proteins.

Hydrogel Formation and pH Responsiveness. The purified proteins were dissolved in an aqueous solution containing 500 μM TCEP at pH 3.8. The protein concentration was determined by absorbance spectroscopy using the Lambert−Beer law at 280 nm. The theoretical extinction coefficients were obtained from the Expasy server[34] based on the proteins' amino acid sequences. We use lyophilized protein at ≥90−95% purity determined by mass spectrometry and polyacrylamide gel electrophoresis.

Hydrogelation started from solutions of ASCc and CARD-peptide at 0.3 mM, ASC at 0.5 mM, and CARD−CARD at 0.3 and 0.9 mM. All hydrogels were formed by slowly increasing the pH from 3.8 to 6.8. Basification was done by stepwise addition of small volumes (2.5−4 μL) of dilute solutions of NaOH (0.1 M) to the concentrated protein solutions. Incubation periods of 5 to 10 min followed each basification step to allow the formation of the hydrogel network over time. The slow basification process starts at pH 3.8 once the CARD and PYD domains are properly folded.[30] The small volumes of the NaOH solution must be pipetted into the center of the protein solution for an even distribution. The solutions are swirled and set aside for 5 min. The pH is monitored after each incubation time with a microelectrode until the pH value reaches 4.8. Subsequent pH increase is achieved by adding approximately 2 μL of 0.05 M NaOH. The flowability of the protein solution decreases at pH > 5. At this point, the incubation time increases to 10 min. The solutions are gently swirled to prevent disruption of the hydrogel network up to the required pH of 6.8. The hydrogelation process for ASC is slower to prevent precipitation. For ASC hydrogelation, the pH is increased at a rate of 0.5 pH units every 120 min. Hydrogel formation and behavior were not studied at pH > 6.8. Changes in the proteins' electrostatic surfaces are not expected in the pH range from 6.8 to 8.3 becasue no amino acids titrate in this pH interval. In addition, pH values higher than 8.3 (titration of the sulfhydryl in the cysteine side chain) could lead to protein unfolding.

To test the pH responsiveness of the hydrogels, the pH was decreased in a stepwise manner from 6.8 to 3.8 and further to 2.5. Images were taken at different acidic pH values to show the transition of the hydrogels into solutions with increasing flowability.

Swelling Ratio. Hydrogel swelling ratios were obtained by lyophilization using eq 1

$$\text{S.R.} = \frac{W_w}{W_D} \tag{1}$$

where S.R. is the swelling ratio, and W_w and W_D are the weights of the wet and dry hydrogel, respectively.

The hydrogels formed in glass vials are weighed and then flash-frozen in liquid nitrogen followed by lyophilization. The weights of

https://doi.org/10.1021/acs.biomac.3c00409
Biomacromolecules 2023, 24, 5563−5577

the wet (W_w) and dry (W_D) hydrogels are obtained before and after lyophilization, respectively, by subtracting the weights of the empty lyophilized vials.

Transmission Electron Microscopy (TEM). A volume of 4 μL of the hydrogel was deposited on a 300 mesh Cu TEM grid that had been glow discharged previously. After 10 min incubation, the grid was washed for 10 s in three 40 μL droplets of high-performance liquid chromatography (HPLC) water and stained in three 40 μL droplets of 2% uranyl acetate. After staining the grid for 5 min, the excess staining solution was wiped. Images of the hydrogels were obtained by using a Talos F200C G2 Transmission Electron Microscope with a field emission gun operating at 200 kV. Images were captured with a Ceta 16 M Camera. The open-source software ImageJ with the options "analyze" and "measure" was used to analyze the dimensions of hydrogel filaments and fibrils.

Scanning Electron Microscopy (SEM). On an aluminum specimen mount, lyophilized protein was deposited on conductive carbon adhesive tape. Samples were coated for 40 s with a gold sputter coater at a vacuum of 0.07 Torr, corresponding to approximately 5 nm gold film. Images were obtained with a Zeiss Gemini 500 Field Emission Scanning Electron Microscope operating at a voltage of 3 kV by using secondary electron detectors. The open-source software ImageJ was used for analysis. The images were first inverted and then the options "analyze particles" and "measure" were used to determine hydrogel pore dimensions with a threshold of 2 μm^2 and no upper limit.

Rheology Experiments. Bulk shear rheological behaviors of ASC, ASCc, CARD-peptide, and CARD−CARD hydrogels at pH 6.8 were investigated using an MCR-302 (Anton Paar) at 25 °C. We used a stainless-steel parallel plate attachment (Anton Paar PP-25, 25 mm diameter) for all experiments. The hydrogels were kept at ∼4 °C and subsequently removed from the cold room and allowed to reach room temperature (∼25 °C). A total of 300 μL of previously cross-linked samples were then carefully taken from a glass vial and loaded onto the center of the bottom steel plate using a plastic spatula. Once in place, the stainless-steel top parallel plate was carefully lowered until the gap reached 500 μm, ensuring that the gel completely filled the cavity. The storage modulus (G') and loss modulus (G'') were then measured as a function of shear strain, γ, and frequency, ω. The storage or the shear modulus G' relates the shear stress that is in phase with the shear strain and provides a measure of the elasticity of the hydrogel network as a function of the forcing frequency or the forcing shear strain. The loss modulus G'' is a measure of the effective dissipation due to viscous friction in the hydrogel. Viscoelastic effects manifest as a phase lag between shear strain and shear stress. Tests were conducted in a humidity chamber to minimize solvent evaporation from the hydrogel samples.

The storage and loss moduli were independently measured by using frequency sweeps and shear strain sweeps. The frequency dependence of G' and G'' was investigated by subjecting the sample to a small amplitude oscillation. The angular frequency, ω, varied between 0.1 and 200 rad/s. The amplitude of the shear strain γ was held constant at 1%, consistent with previously published parameters.[35] Next, the strain response of G' and G'' was investigated by subjecting new samples to oscillatory shear at constant angular frequency ω of 6.28 rad/s (equivalent to 1 Hz) while varying the strain amplitude γ, from 0.1 to 100%.[35] Two independent experiments for frequency and strain responses were performed per hydrogel, corresponding to 16 hydrogel samples.

Circular Dichroism (CD). Far-UV-CD spectra for pH-reversibility experiments were recorded from 190 to 250 nm with 1 nm resolution and 1 nm bandwidth at 293 K on a Chirascan CD spectrometer from Applied PhotoPhysics Ltd. (U.K.) equipped with a temperature controller system. Rectangular cuvettes with 1 and 0.2 mm path lengths were used to hold the protein samples at pH 3.8 and 6.8, respectively.

CD spectra for the temperature ramp experiments were acquired with the same parameters from 278 to 368 K every 5 K with a cuvette of 1 mm path length. The spectrum of the buffer was subtracted from the proteins' CD spectra, and baseline correction was applied.

Samples for pH-reversibility experiments were prepared initially at protein concentrations close to 50 μM in 500 μM TCEP at pH 3.8. All concentrations were determined by absorbance spectroscopy. CD spectra were acquired for all protein samples at pH 3.8 in a 1 mm quartz cuvette. Subsequently, the pH was increased to 6.8, resulting in protein precipitation. All samples were centrifuged for 1 min at 14,000 rpm to collect the supernatants. CD spectra of the supernatants were acquired at pH 6.8 in a 0.2 mm quartz cuvette. The pH of the protein samples was decreased back to 3.8, and CD spectra were acquired to test for reversibility.

Samples to determine protein stability were prepared at a 20 μM protein concentration in 500 μM TCEP at pH 3.8. The protein samples were unfolded gradually by temperature increase from 278 to 368 K in 5-degree intervals. CD spectra were acquired in a 1 mm quartz cuvette at each temperature point. The ellipticity at 222 nm characteristic of α-helices was plotted as a function of temperature. The resulting plots were fit to a two-state model of protein folding using MATLAB to determine the unfolding temperature as previously described.[36,37] All fittings resulted in R^2 values > 0.99.

RESULTS

Protein Design for Hydrogel Formation Based on the Structure and Oligomerization Properties of ASC. Previously, we showed that full-length ASC polymerizes into filaments and filament bundles via homotypic protein−protein interactions mediated by its two oligomerization domains, PYD and CARD.[30−32] Based on the analysis of TEM micrographs, we reported that these filaments are ∼7 nm wide and reach lengths of 1 μm.[38] The filaments assemble laterally, forming bundles of 2 to 7 filaments. Oligomerization is not restricted to the full-length protein, as we have shown that ASC's individual domains are capable of polymerizing into filaments as well.[38] Using solution NMR, we found that homotypic CARD−CARD binding affinity is slightly higher than that of PYD−PYD binding.[38,39] We also demonstrated that ASC interactions are pH-dependent. ASC is properly folded and monomeric at pH 3.8; however, it precipitates at higher pH values.[31] The three-dimensional (3D) structure of ASC (Figure 1A) reveals the protein's electrostatic surface composed of positively and negatively charged patches, as well as some nonpolar regions involved in ASC filament formation.[31] At low pH, the negative charges are neutralized, thus shielding the electrostatic interactions and shifting the monomer−oligomer equilibrium toward the monomeric species. Upon pH increase, deprotonation results in a larger number of negative charges leading to favorable intermolecular electrostatic interactions that are essential for the noncovalent polymerization of the protein.[38]

Recently, a short peptide inspired by the amino acid sequence of the ASC-PYD domain with the addition of the self-assembly moiety Nap-FF (a naphthalene aromatic ring followed by two phenylalanine amino acids) has been shown to form nanofibers.[40] Based on these studies and considering the polymerization capabilities of ASC and its domains, we hypothesized that full-length ASC could also form hydrogels. This is an important question because there are almost no examples of globular proteins and domains in their native conformation that are known to form hydrogels. To test our hypothesis, we aimed at creating hydrogels solely composed of natural ASC. In addition, ASC has several isoforms with similar structural characteristics.[33] Thus, we speculated whether the isoforms could also form hydrogels. We specifically focused on the isoform ASCc that has been shown to inhibit, rather than activate the inflammasome.[33] The inhibition mechanism is not known, but it has been postulated that ASCc might interfere

https://doi.org/10.1021/acs.biomac.3c00409
Biomacromolecules 2023, 24, 5563−5577

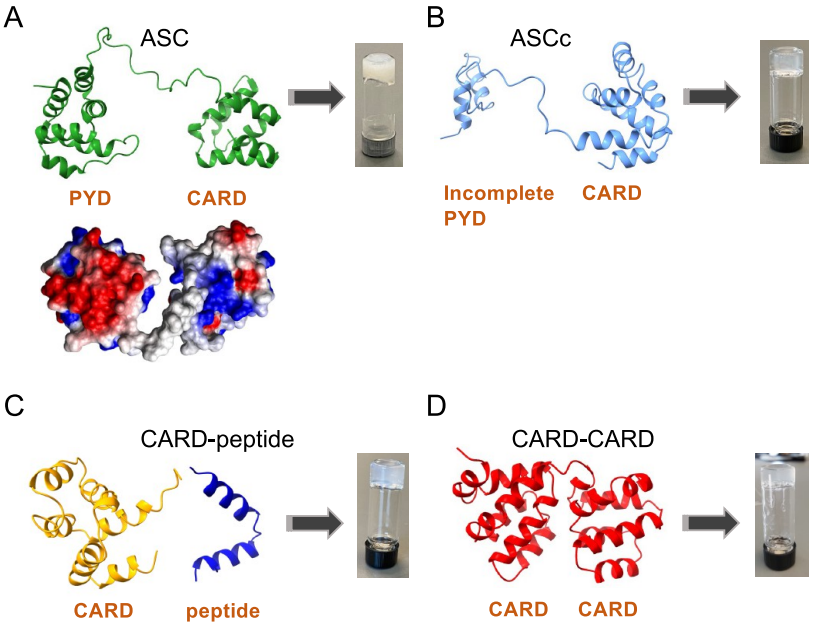

Figure 1. Three-dimensional structures of the proteins used for hydrogel formation. (A) ASC experimental structure determined by solution NMR.[31] Top: ribbon diagram depicting the polypeptide backbone; bottom: electrostatic surface showing negatively and positively charged patches in red and blue, respectively; (B) ASCc structural model; (C) CARD-peptide model: CARD structure from ASC[31] and peptide structural model; (D) CARD−CARD model structure. Images of the respective hydrogels formed by these proteins are shown next to each model structure. The structural models were created with I-Tasser.[41] The ribbon diagrams of the proteins' backbone were done with ChimeraX.[42]

with ASC self-assembly thus disrupting the formation of the inflammasome.[33]

To gain an understanding of the conformation of ASCc, we created a structural model with the program I-Tasser that uses a database of experimental 3D protein structures.[41] The model indicates that ASCc likely carries an intact CARD and an incomplete PYD (Figure 1B). ASCc will likely polymerize despite the incomplete PYD since we demonstrated that ASC-CARD polymerizes into filaments[38] and the amino acid sequence of ASCc-CARD shares 100% identity with ASC-CARD.[33] To determine the role of the incomplete PYD in the potential hydrogelation of ASCc, we created an artificial protein carrying ASCc-CARD and attempted hydrogelation in the presence and absence of a synthetic peptide comprising the residual PYD (Figure 1C). Finally, we engineered a completely artificial protein carrying two CARD domains in tandem to study hydrogelation (Figure 1D). We chose the CARD domain due to the stronger affinity for homo-oligomerization.[38,39] The names we use henceforth for these ASC-inspired proteins refer to their respective molecular compositions: ASC, ASCc, CARD-peptide, and CARD−CARD (Figure 1).

Hydrogelation Process of ASC-Inspired Proteins Is pH-Dependent. ASC, ASCc, and the PYD and CARD domains oligomerize and precipitate when the solution pH is increased quickly from acidic to neutral values. Our data show that massive precipitation occurs by a pH increase in the 0.3−1 mM protein concentration range. However, a slow and tightly controlled basification leads to the formation of hydrogels (Figure 2). The 3D NMR structure of ASC was determined at pH 3.8 demonstrating that the protein is properly folded adopting the six-helix bundle motif of the Death Domain fold.[31,32,43] Thus, the hydrogelation process must start at this pH to ensure the formation of the correct protein electrostatic surface required for proper oligomerization. The pH value is gradually increased to pH 4.8 in three to four 5 min steps. Basification is set at a significantly slower pace after pH 4.8, requiring multiple steps spaced by 10 min. The slow pH-increase process for hydrogelation takes approximately 4 h.

Upon pH increase to 6.8, the protein solutions thicken, suggesting increased viscoelastic characteristics and finally resulting in hydrogel formation upon overnight incubation at room temperature. The first indication of hydrogelation is the decreased flowability and solid-like appearance of the solution, which fails to flow to the bottom of the vial when inverted (Figure 2). Reaching a pH of 6.8 is important for hydrogel consistency as overnight incubation at a more acidic pH (e.g., pH 5.5) leads to more flowable hydrogels (Figure 2A). This result points to the importance of the negatively charged regions of the protein surface for polymerization and hydrogel formation, resulting from the deprotonation at pH values higher than 5.5. Overnight hydrogelation was obtained for ASC and ASCc (0.5 and 0.3 mM protein concentration, respectively). We failed to form ASC hydrogels at 0.3 mM, which suggests that the protein concentration is an important factor in hydrogelation. In addition, the capability of ASC and ASCc to form hydrogels implies that the complete PYD (Figure 1) is not required and indicates that hydrogelation might be possible for constructs containing only the CARD domain.

Thus, we engineered a CARD-only construct (no PYD or incomplete PYD linked) and tested its hydrogelation capabilities. The CARD-only protein solution (0.3 mM) thickened upon a slow pH increase after overnight incubation (Supporting Figure S2). Additional incubation time and basification were required for hydrogelation. In contrast, increasing the concentration of the CARD-only protein solution to 0.5 mM did not improve the hydrogelation capabilities. The CARD-only hydrogel showed more flowability compared to ASC and ASCc hydrogels as it deforms when inverted (Supporting Figure S2). This was a surprising

https://doi.org/10.1021/acs.biomac.3c00409
Biomacromolecules 2023, 24, 5563−5577

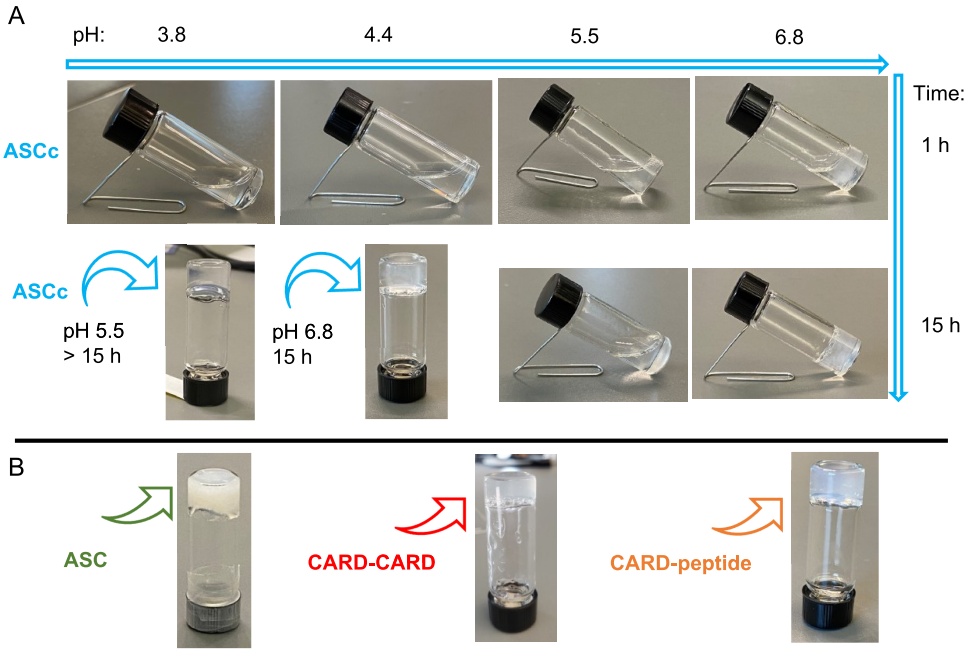

Figure 2. pH-Dependent hydrogelation of ASC, ASCc, CARD-peptide, and CARD−CARD. (A) Hydrogelation process of ASCc (0.3 mM) as a function of pH increase and time. (B) Hydrogels formed by ASC (0.5 mM), CARD−CARD (0.9 mM), and CARD-peptide (0.3 mM) by analogous pH increase and overnight incubation.

result, as ASCc with a CARD and an incomplete PYD is capable of overnight hydrogelation. Therefore, we tried to emulate this structure by mixing equimolar concentrations of the CARD-only protein with a synthetic peptide comprising the incomplete PYD domain of ASCc (hydrogel: CARD-peptide at 0.3 mM) (Figure 1C). This heterotypic interaction facilitated overnight hydrogel formation of the CARD-only construct with the synthetic peptide (Figure 2B). The presence of a heterotypic interaction is not surprising because this type of binding between Death Domains has been reported, although is less common than homotypic binding.[44] Nonetheless, the interaction between the CARD-only protein and the peptide does not involve two full Death Domains.

We also tested the behavior of CARD-only in the presence of minor amounts of the peptide instead of equimolar concentration, observing that hydrogelation is not complete after overnight incubation, but the hydrogel eventually forms after several days. This result indicates that equimolar amounts of the peptide emulating the incomplete PYD promote hydrogelation. The CARD-peptide hydrogel is an example of the possibility of forming a hydrogel with two separate molecular components. However, the hydrogelation process is significantly perturbed when one of the components is missing. The capability of CARD-only and CARD-peptide to form hydrogels indicates that the linker connecting the two domains in ASC and ASCc (Figure 1) is not essential for hydrogel formation. However, it has been demonstrated that the linker tethering the two Death Domains plays an important role in the initial stages of the oligomerization kinetics of ASC isoforms.[45,46]

The CARD-peptide hydrogel is an artificial construct designed based on the structure of ASCc (i.e., the CARD of ASCc and a synthetic peptide comprising the amino acids sequence of the incomplete PYD) (Figure 1). To test whether another artificial construct could form a hydrogel, we engineered the protein CARD−CARD, with two CARD domains in tandem connected by a short linker. The CARD domain was selected for this design to maximize hydrogelation capabilities as the CARD shows a slightly higher affinity for self-association than the PYD.[38,39] The CARD−CARD protein is also capable of hydrogelation following an analogous process of pH increase and overnight incubation of protein solutions at concentrations of 0.3 and 0.9 mM (Figure 2B). This result suggests that the PYD can be replaced by an additional CARD for protein hydrogelation. The CARD−CARD hydrogel at 0.3 mM shows higher flowability compared to the solution at 0.9 mM (Supporting Figure 3 and Figure 2, respectively), indicating that the protein concentration is an important factor in hydrogelation as observed for ASC hydrogels.

It is important to note that the isoelectric point (pI) of the proteins is close to neutral pH and thus very similar to the final pH value for optimum hydrogelation. The pIs are 6.80 (ASC), 7.14 (ASCc), and 7.14/6.04 for CARD and peptide, respectively, and 6.83 (CARD−CARD). As commonly observed in globular proteins, the number of positively and negatively charged amino acids (Arg, Lys, and Asp and Glu, respectively) at neutral pH in the proteins studied is very similar. The positive and negative charges, respectively, are 23, 24 (ASC); 16, 16 (ASCc); 11, 11 and 5, 5 (CARD-peptide); and 22, 21 (CARD−CARD). Thus, the pH dependence of the hydrogelation process is not related to the number of charges *per se*, but to the clustering of these charges in the protein electrostatic surface (Figure 1A). Nonetheless, we reported previously that hydrophobic interactions also play an important role in ASC self-association.[39]

All four hydrogels are relatively soft and can be easily deformed with a pipet tip or a spatula. This is an expected result, as ASC-inspired hydrogels are assembled by physical cross-linkages resulting from electrostatic interactions and from the hydrophobic effect. These weak interactions explain why the hydrogelation process is reversible. Decreasing the pH back to acidic values regenerates the liquid protein solutions

https://doi.org/10.1021/acs.biomac.3c00409
Biomacromolecules 2023, 24, 5563−5577

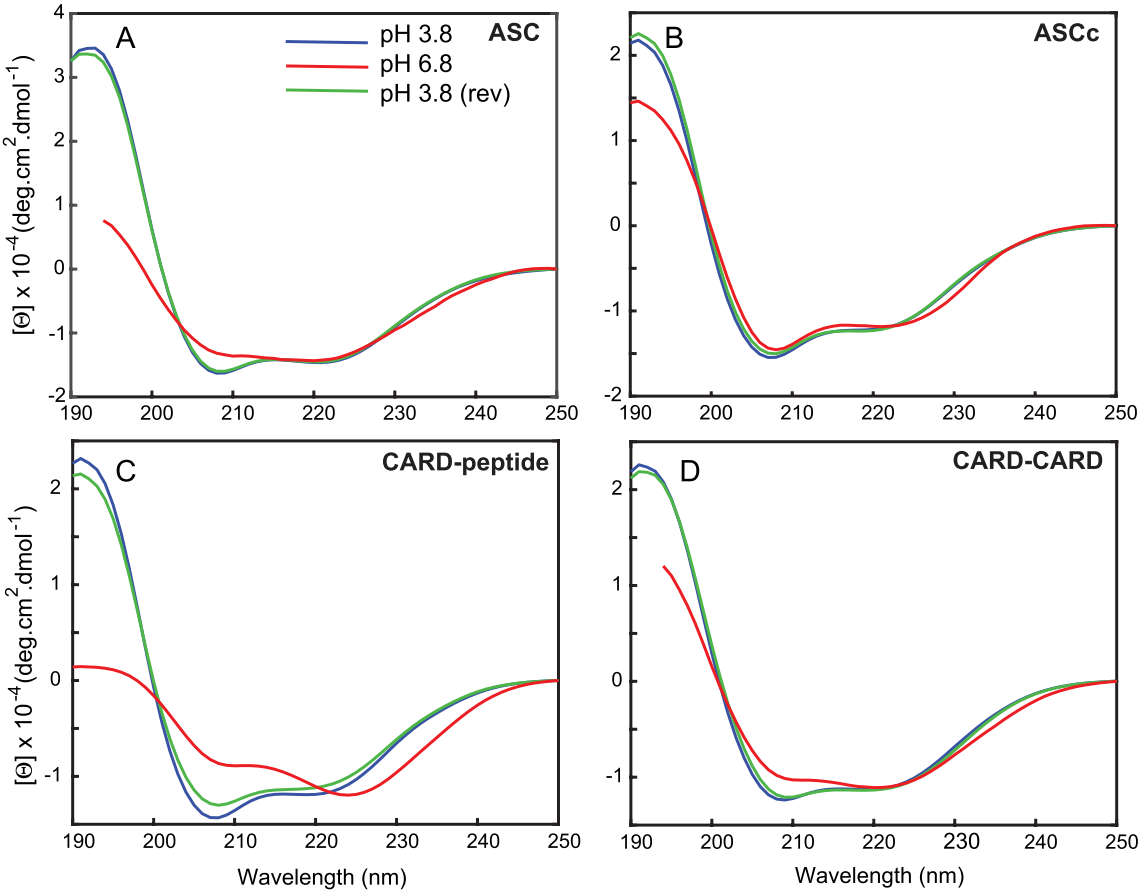

Figure 3. ASC-inspired proteins adopt α-helical structures at pH 3.8 and 6.8. Far-UV circular dichroism spectra of ASC-inspired protein samples at pH 3.8 (blue), 6.8 (red), and back at pH 3.8 (green). The spectra at pH 6.8 and the reversibility test at 3.8 were multiplied by different factors to account for protein precipitation and overall protein loss, respectively. The signal close to 190 nm is not shown for ASC and CARD−CARD due to high noise likely caused by the longer path length and the absorption of the buffer.

(Supporting Figure 4). A small amount of protein material does not completely dissolve after hydrogel disassembly by decreasing the pH to 3.8, resulting in slightly hazy solutions. Further acidification to 2.5 enhances the dissolution of protein oligomers as demonstrated by the decrease in haziness (Supporting Figure 4). Upon acidification, the negatively charged amino acids are neutralized, thus shielding the electrostatic interactions with the positively charged regions of the protein surface, leading to oligomer dissociation.

We performed circular dichroism (CD) experiments with a 2-fold purpose: (1) to show that the proteins are folded at both acidic and close to neutral pH values (pH 3.8 and 6.8, respectively), thus retaining their secondary structure upon pH change and (2) further demonstrate pH-reversibility. The CD spectra were acquired for all protein solutions at pH 3.8, subsequently after increasing the pH to 6.8, and upon acidification back to 3.8.

At pH 3.8, all spectra show two minima at ∼208 and ∼222 nm characteristic of the α-helical structure, as expected based on the NMR studies on ASC and its individual domains at atomic resolution[31,32,38,39] (Figure 3). The absolute value of the minimum at 208 nm is larger than that at 222 nm, whereas the opposite is typical for α-helices. This result might reflect the contribution of other amino acidic fragments, such as linkers connecting the two domains. Previously reported CD data of helical peptides derived from the PYD domain of ASC show the same feature.[47] However, the CD spectra of isolated helical peptides typically show 208 nm minima lower than the 222 nm.[48]

As expected, the proteins precipitate significantly after the pH is increased to 6.8. Thus, a cuvette with a path length 5 times lower was required to acquire the CD spectra of the soluble fractions due to the low protein concentration. The CD spectra of the proteins at pH 6.8 are characteristic of the α-helical structure with two minima at ∼208 and 222 nm (Figure 3). Interestingly, the absolute value of the minimum at 208 nm becomes smaller than that at 222 nm for all proteins except ASCc. An effect that is significantly pronounced for the CARD-peptide mixture (Figure 3C). This feature in CD spectra has been observed in coiled coils and is attributed to the formation of helix−helix interactions.[48,49]

The 3D structures of CARD and PYD domains polymerized forming filaments under physiological pH conditions have been determined by cryo-EM showing that the proteins conserve the six-helix bundle motif.[50,51] However, these studies identified conformational differences compared to the isolated structures[31,39] due to the interactions forming the polymer. Thus, the change in the CD spectra of ASC-inspired proteins could be explained by the presence of more prominent interhelical interactions at pH 6.8, as this pH favors protein self-association and polymerization.[39,45,46]

The CD spectrum of the CARD-peptide at pH 6.8 also shows a larger red shift of the minimum at 222 nm, suggesting more pronounced structural arrangements. In contrast, the CD

https://doi.org/10.1021/acs.biomac.3c00409
Biomacromolecules 2023, 24, 5563−5577

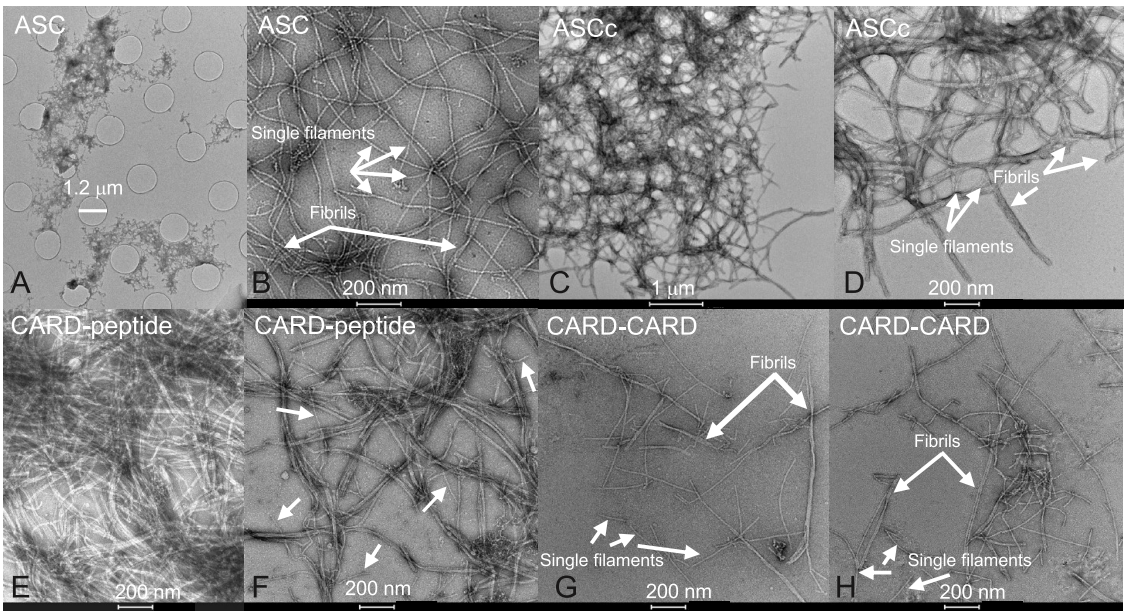

Figure 4. Intricate network of protein filaments and fibrils form the structural scaffold of ASC-inspired hydrogels. Transmission electron micrographs of ASC (A, B), ASCc (C, D), CARD-peptide (E, F), and CARD−CARD (G, H) hydrogels. Arrows point to single filaments and fibrils, as indicated in each panel. For the CARD-peptide hydrogel, panel (E) shows multiple fibrils, and the arrows in panel (F) point to individual filaments. Scale bar dimensions are indicated. The contrast in panel (E) was modified with respect to the original image to show the fibrils with more clarity.

Table 1. Analysis of Filaments and Fibrils formed by ASC-Inspired Hydrogels[a]

	Hydrogel			
	ASC	ASCc	CARD-peptide	CARD−CARD
filament width	7.2 ± 0.5 nm	7.0 ± 0.9 nm	7.3 ± 0.5 nm	7.4 ± 0.5 nm

[a]Data from a total of 50 filaments per hydrogel.

spectra of ASCc show little change between pH 3.8 and 6.8, except for a clear red shift of the 222 nm minimum at the more basic pH. We can only speculate whether ASCc polymerization might require fewer interhelix contacts or the presence of the linker and the residual PYD interfere to some extent with these interactions.

Overall, the structural studies by CD indicate that the secondary structure of the proteins is α-helical under the conditions required for hydrogelation. In addition, the characteristics of the original spectra are recovered after decreasing the pH back to 3.8 demonstrating reversibility (Figure 3). The CD spectra of ASC at pH 3.8 and 6.8 are analogous to the spectra of the other proteins. Thus, we can conclude all proteins are properly folded under these conditions as the atomic resolution structure of ASC at pH 3.8 shows two six-helix bundle motifs for the PYD and CARD domains, respectively.[31] These results indicate that ASC-inspired hydrogels are formed by the self-assembly of proteins in their native structures.

Finally, ASC-inspired hydrogels are not completely transparent, showing different degrees of opaqueness, with the ASC hydrogel being opaque white. The various shades of white suggest different levels of reflected and scattered light, which could be related to the structural characteristics of the hydrogels. Slight precipitation of the protein material embedded in the hydrogels could cause haziness as well. To better understand the structure of ASC-inspired hydrogels, we used transmission (TEM) and scanning (SEM) electron microscopy.

Structural Scaffold of ASC-Inspired Hydrogels Is Formed by an Intricate Network of Protein Filaments and Fibrils. We have previously shown that ASC and other isoforms polymerize into filaments and filament bundles in the absence of hydrogelation.[38,45,46] Therefore, this type of macrostructure is expected to be the essential structural unit of ASC-inspired hydrogels. However, the hydrogelation process could result in modification of these filaments, thus requiring additional analysis by TEM. Because sample thickness is key to obtaining high-quality images, we inserted a micropipet in formed hydrogels to extract a fraction of the hydrogel material. The TEM images of the 4 hydrogels reveal structural units formed by protein filaments and filament bundles (fibrils) and show that all hydrogels form large, entangled filament networks (Figure 4).

These filaments and fibrils were further analyzed to identify potential differences in their dimensions. The analysis of 50 individual filaments per hydrogel indicates that the filaments have similar widths falling in the 6.1−7.9 nm range (Table 1). However, small differences were observed in the frequency of the number of filaments forming fibrils. The analysis of a total of 122 fibrils shows that ASCc and CARD−peptide hydrogels tend to self-assemble into thick bundles composed of 6 and 7 filaments (Figure 5).

ASC-Inspired Hydrogels Have Porous Structures. We have used SEM to characterize the macrostructures of the ASC-inspired hydrogels. Micrographs obtained at different magnifications show that the 4 hydrogels have porous structures, suggesting significant permeablility (Figure 6).

https://doi.org/10.1021/acs.biomac.3c00409
Biomacromolecules 2023, 24, 5563−5577

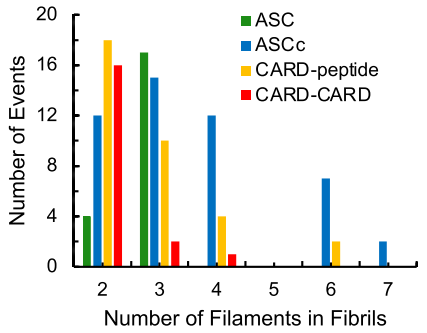

Figure 5. Number of filaments in fibrils formed by ASC-inspired hydrogels. ASCc and CARD-peptide show a slightly higher tendency to form filament bundles composed of 6−7 filaments. Bar height indicates the number of fibrils with the corresponding number of stacked filaments (*X*-axis). Color code is indicated at the top of the figure.

The surfaces of ASC, CARD-peptide, and CARD−CARD appear flaky, whereas the surface of ASCc is more rounded.

Using these images, we performed a pore size analysis to identify similitudes and differences between the hydrogels (Figure 7). The pore size reported here reflects an effective

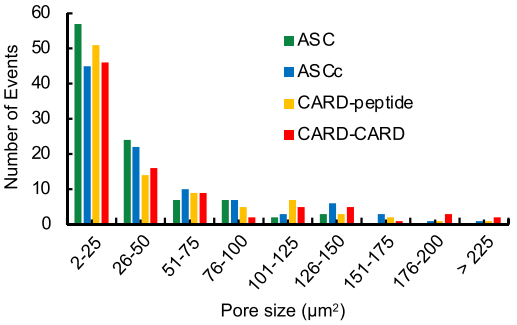

Figure 7. Pore size analysis of ASC-inspired hydrogels. Bar height represents the number of pores with the corresponding area (*X*-axis). Color code is indicated at the top of the figure.

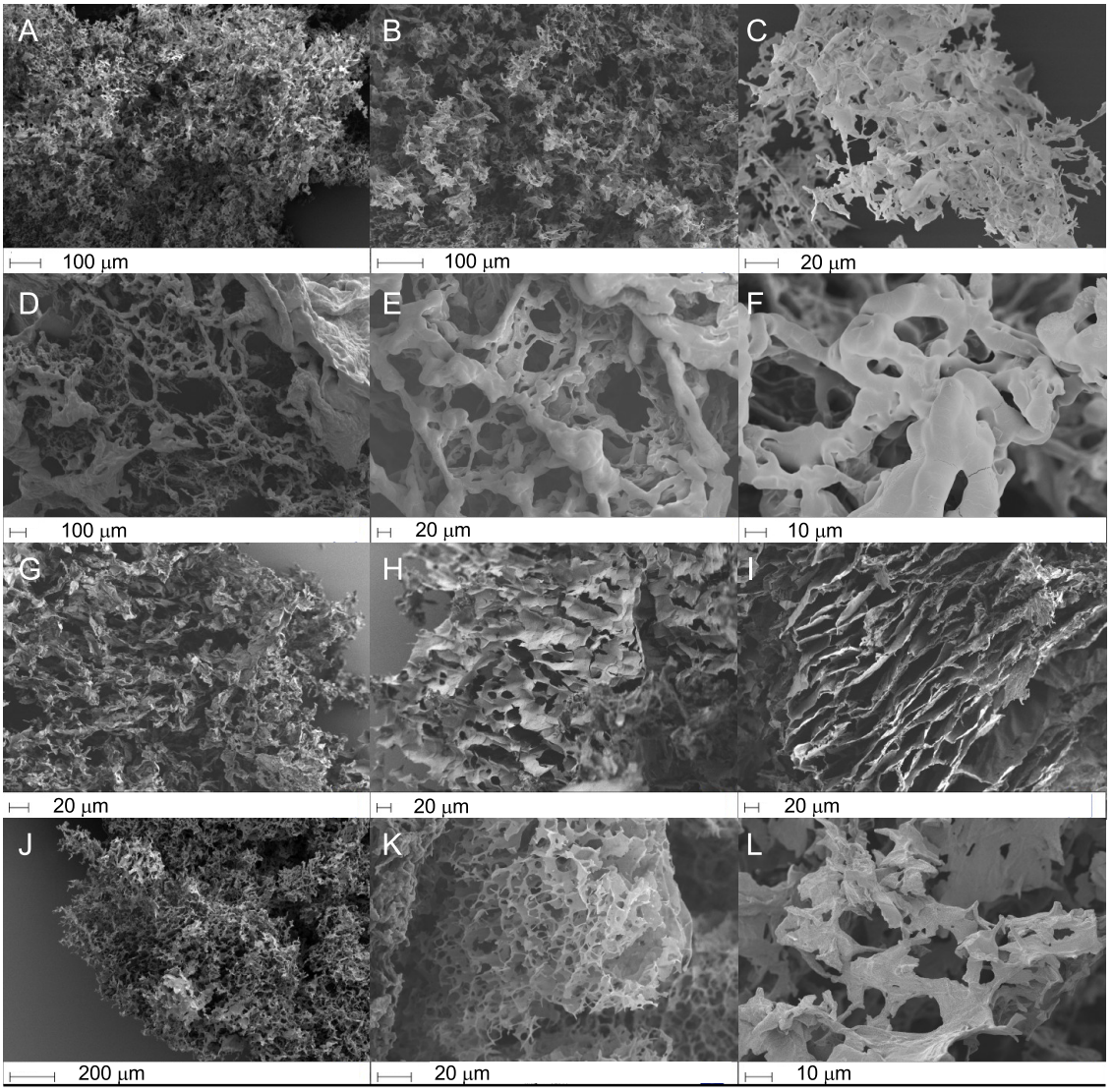

Figure 6. ASC-inspired hydrogels have porous structures. Scanning electron micrographs from secondary electrons at different magnifications of ASC (A−C), ASCc (D−F), CARD-peptide (G−I), and CARD−CARD (J−L) hydrogels. Scale bar dimensions are indicated.

https://doi.org/10.1021/acs.biomac.3c00409
Biomacromolecules 2023, 24, 5563−5577

void size and is therefore related to the effective permeability of the hydrogel. The analysis of 380 pores up to 225 μm^2 shows that the 4 hydrogels tend to form pores smaller than 25 μm^2, pores sizes in the 25−50 μm^2 range are also abundant, although less prominent, and sizes larger than 100 μm^2 are increasingly infrequent. ASC is the only hydrogel for which pores in the 150−225 μm^2 range were not observed (Figure 7).

To connect the pore size distributions with the capability to swell in the presence of water, we measured the hydrogel swelling ratios using lyophilization. The swelling ratios of ASC-inspired hydrogels fall in the range of 77 to 156 (Table 2).

Table 2. Swelling Ratios of ASC-Inspired Hydrogels[a]

	hydrogel			
	ASC	ASCc	CARD-peptide	CARD−CARD
swelling ratio	78 ± 1[b]	117 ± 26	123 ± 33	120 ± 4

[a]Values represent a minimum of two measurements. [b]All hydrogels at 0.3 mM except ASC hydrogel at 0.5 mM.

These values are in accord with physically cross-linked hydrogels that typically do not increase their volume as much as chemically formed hydrogels.[5] The smaller swelling ratio observed for ASC could be related to the higher protein concentration used to form the hydrogels. In addition, the precision in the swelling ratio measurements varies significantly from 1 to 33. Overall, ASC-inspired hydrogels do not show significant differences in their capacity to absorb water.

Viscoelastic Properties of ASC-Inspired Hydrogels. To characterize the viscoelastic response of ASC, ASCc, CARD-peptide, and CARD−CARD at pH 6.8, we conducted shear rheology measurements. The log−log curves of the storage modulus (G') and loss modulus (G'') as a function of angular frequency (ω) and shear strain (γ) are shown in Figures 8 and 9, respectively. The larger values of G' compared to G'' indicate the presence of stable hydrogels with some ability to withstand shear deformations. For the experiments conducted at various values of the angular frequency, our results reveal that the G' and G'' values slightly increase with increasing frequency within the frequency range tested, indicating that the hydrogels become stiffer (Figure 8). The shear strain sweep tests showed different rheological responses of the hydrogels. All hydrogels show a linear viscoelastic region up to shear strains of approximately 10%, indicating a predominantly elastic response without stiffening (Figure 9). The characteristic crossover point, where the two moduli are approximately the same, quantifies the value at which the rheological response of the hydrogel transitions from predominantly elastic behavior to predominantly liquidlike viscous behavior. We find that this characteristic crossover point is construct-dependent. Specifically, these crossover points are 7.5 Pa @ 15.8%, 3.4 Pa @ 39.7%, 17.8 Pa @ 19.9%, and 3.2 Pa @ 31.5% for ASC, ASCc, CARD-peptide, and CARD−CARD, respectively. These different crossover points indicate that ASCc and CARD−CARD

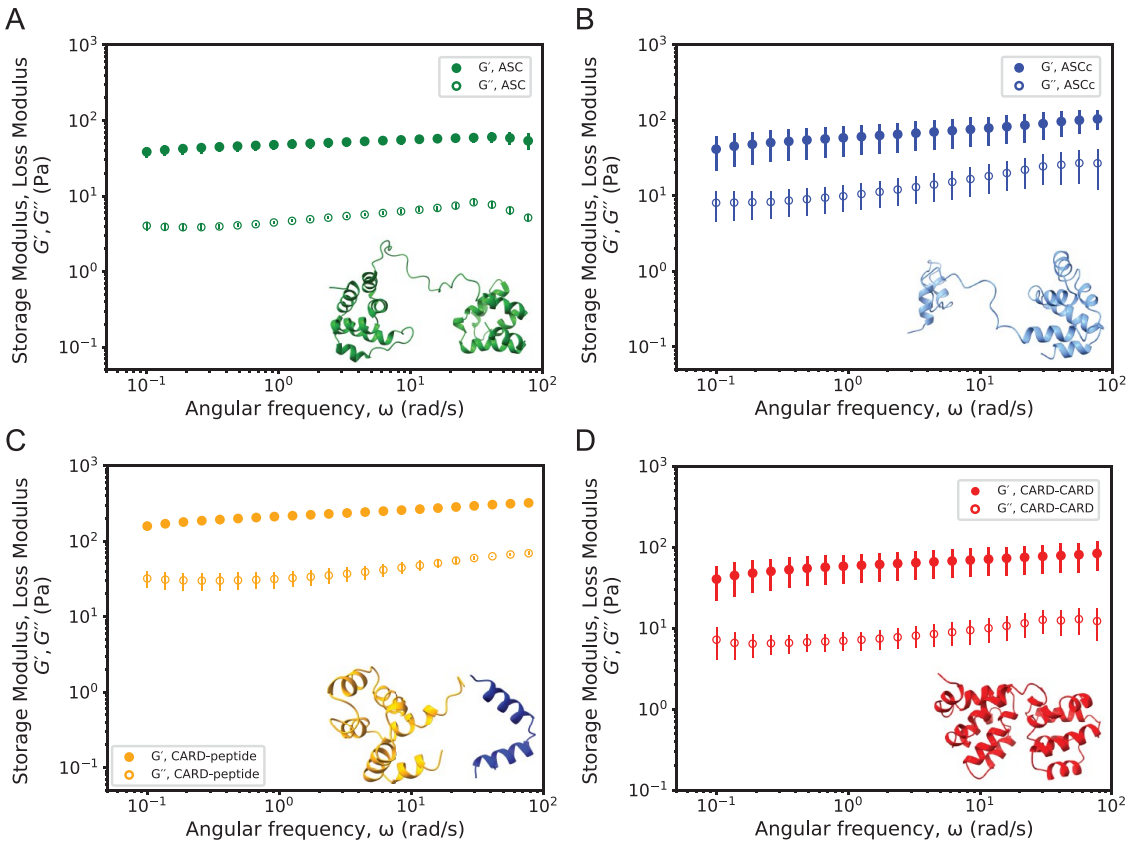

Figure 8. Viscoelastic response of ASC-inspired hydrogels as a function of shear strain. Log−log plot of storage (G', solid symbols) and loss (G'', open symbols) moduli as a function of shear strain at a constant frequency of 1 Hz (6.28 rad/s) for (A) ASC (0.5 mM), (B) ASCc (0.3 mM), (C) CARD-peptide (0.3 mM), and (D) CARD−CARD (0.3 mM). Data reported for each condition are the average of two independent measurements. Error bars represent the standard error of the mean.

https://doi.org/10.1021/acs.biomac.3c00409
Biomacromolecules 2023, 24, 5563−5577

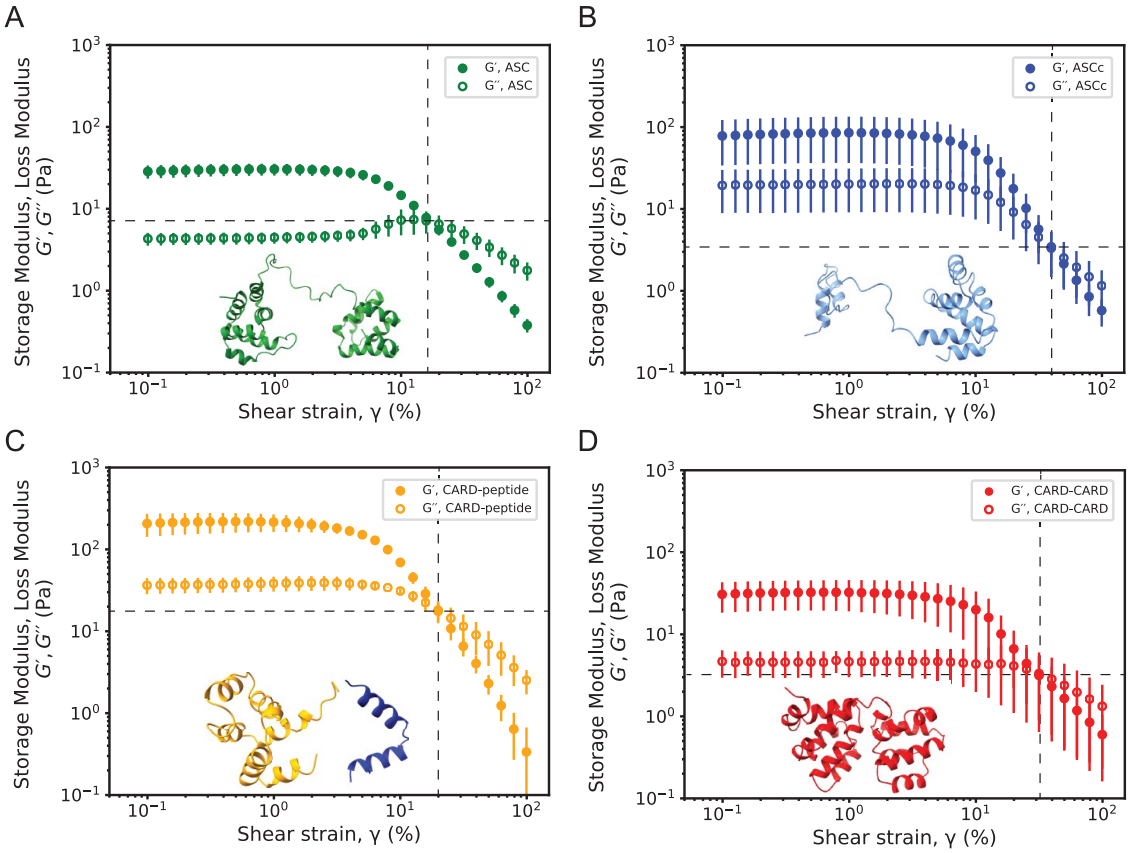

Figure 9. Viscoelastic response of ASC-inspired hydrogels as a function of angular frequency. Log−log plot of storage (G', solid symbols) and loss (G'', open symbols) moduli as a function of angular frequency at 1% shear strain for (A) ASC (0.5 mM), (B) ASCc (0.3 mM), (C) CARD-peptide (0.3 mM), and (D) CARD−CARD (0.3 mM). Data reported for each condition is the average of two independent measurements. Error bars represent the standard error of the mean.

Table 3. Initial Storage (G') and Loss (G'') Moduli, and Shear Strain at the Crossover Modulus ($G' \approx G''$) for ASC-Inspired Hydrogels[a]

	hydrogel[b]			
	ASC	ASCc	CARD-peptide	CARD−CARD
frequency sweep (Pa)	$G' = 38 \pm 6$	$G' = 41 \pm 20$	$G' = 158 \pm 37$	$G' = 40 \pm 18$
	$G'' = 4.0 \pm 0.5$	$G'' = 8 \pm 3$	$G'' = 32 \pm 8$	$G'' = 7 \pm 3$
shear strain sweep (Pa)	$G' = 29 \pm 5$	$G' = 78 \pm 44$	$G' = 207 \pm 65$	$G' = 31 \pm 12$
	$G'' = 4.3 \pm 0.8$	$G'' = 19 \pm 10$	$G'' = 36 \pm 8$	$G'' = 5 \pm 2$
crossover moduli $G' \approx G''$ (Pa)	7.5 @ 15.8%	3.4 @ 39.7%	17.8 @ 19.9%	3.2 @ 31.5%

[a]Mean and standard error of the mean. [b]All hydrogels at 0.3 mM except ASC at 0.5 mM.

maintain their integrity over larger shear strain values, approximately twice the strain compared to ASC and CARD-peptide.

The G' and G'' values obtained are comparable for the ASC, ASCc, and CARD−CARD hydrogels, whereas the CARD-peptide hydrogel shows significantly higher values of G' (Table 3). For CARD-peptide, the rheology data can be correlated with circular dichroism data at pH 6.8, showing the largest difference between the minima at 208 and 222 nm. Taken together, this suggests stronger or more abundant interhelical interactions that could result in higher G' values.

The hydrogelation processes in ASC-inspired hydrogels depend on cross-linkages formed by physical interactions between the globular domains rather than chemical (covalent) interactions, which are common in nonbiological, synthetic hydrogels. The type of cross-linkage has an important impact on the hydrogel's mechanical properties; physically cross-linked hydrogels are less resistant to mechanical forces compared to covalently linked hydrogels.[5] Overall, ASC-inspired hydrogels show lower storage and loss moduli compared to the positively and negatively charged peptides derived from ASC helices with self-assembling moieties, which show G' values in the 200−400 Pa range.[35] The slight protein precipitation as evidenced by the hazy appearance of the hydrogels could lead to overall lower values of the storage modulus due to the lower number of molecules in the network.

Stability of ASC-Inspired Proteins. To better understand the viscoelastic properties of ASC-inspired hydrogels, we studied the stability of the different proteins by thermal denaturation. Changes in protein structure upon temperature-induced unfolding were monitored by circular dichroism (Figure 10). All protein solutions at pH 3.8 were subjected to a

https://doi.org/10.1021/acs.biomac.3c00409
Biomacromolecules 2023, 24, 5563−5577

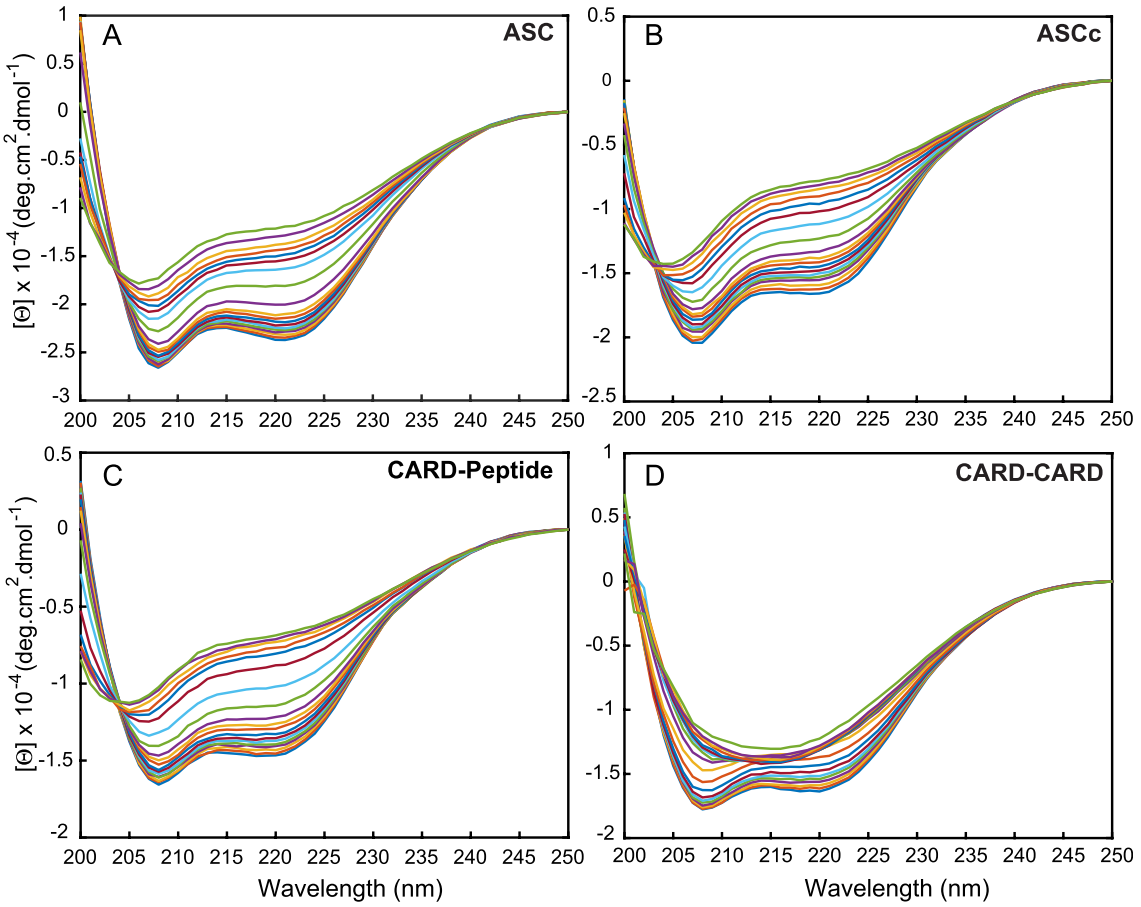

Figure 10. Thermal denaturation of ASC-inspired proteins. Far-UV circular dichroism spectra of (A) ASC, (B) ASCc, (C) CARD-peptide, and (D) CARD−CARD protein solutions at pH 3.8 as a function of temperature from 278 to 368 K. The blue lines with the largest absolute values of the minima at ∼208 and 222 nm correspond to 278 K. These values decrease as the temperature increases up to 368 K corresponding to the green line at the top of the spectra.

temperature ramp from 278 to 368 K. The CD spectra at 278 K are analogous to the spectra at 293 K and pH 3.8 shown in Figure 3; however, the minima at ∼208 and 222 nm are more pronounced at the lower temperature, indicating stabilization of the α-helical structure (Figure 10). As the temperature increases, the absolute values of the minima decrease and shift to lower wavelengths for ASC, ASCc, and CARD-peptide. In contrast, CARD−CARD shows a different behavior. The minima at 208 and 222 nm undergo red and blue shifts, respectively. At temperatures ≥ 338 K, the CD spectrum of CARD−CARD shows a single broad minimum at ∼215 nm. The CD spectra at 293 K of the ASC, ASCc, and CARD-peptide protein solutions before and after thermal denaturation are superimposable (data not shown). This result indicates the reversibility of the unfolding process. Interestingly, the pre- and post-unfolding CD spectra of CARD−CARD are not superimposable, suggesting that the process is irreversible.

Mean residue ellipticity values at 222 nm plotted as a function of temperature were fit to a two-state model as previously described[36,37] to determine the melting temperature of the different proteins (Figure 11). The protein unfolding studies reveal that CARD−CARD and CARD-peptide are the least and most stable proteins, respectively, whereas the natural isoforms ASC and ASCc show intermediate stabilities.

CONCLUSIONS

We have shown here that globular folded proteins and domains of the Death Domain superfamily form noncovalent, pH-responsive hydrogels. Our findings provide one of the very few examples of hydrogels created by the self-assembly of globular proteins and domains in their native conformation without the need to use any proteinaceous or nonproteinaceous cross-linkages. The hydrogelation process of Death Domains is mainly controlled by the solution pH; however, other factors, such as molecular composition, protein concentration, and hydrogelation time, play important roles. In this work, we have studied the hydrogelation of the Death Domain member ASC, carrying a PYD and a CARD. We have shown that its isoform, ASCc, which bears the CARD but lacks a complete PYD, is also capable of forming hydrogels. We have demonstrated the general hydrogelation capabilities of the Death Domains, PYD and CARD, by forming hydrogels with designed protein constructs based on these domains. Thus, our work opens the door to further studies on the hydrogelation capabilities of other members of the Death Domain superfamily, such as Death Effector Domain (DED) and Death Domain (DD). Death Domain proteins control the formation of large signaling complexes, such as the inflammasome. Therefore, one of their main functions is to participate in protein−protein interactions and oligomerization. This behavior poses significant challenges for biophysical and biochemical studies,

https://doi.org/10.1021/acs.biomac.3c00409
Biomacromolecules 2023, 24, 5563−5577

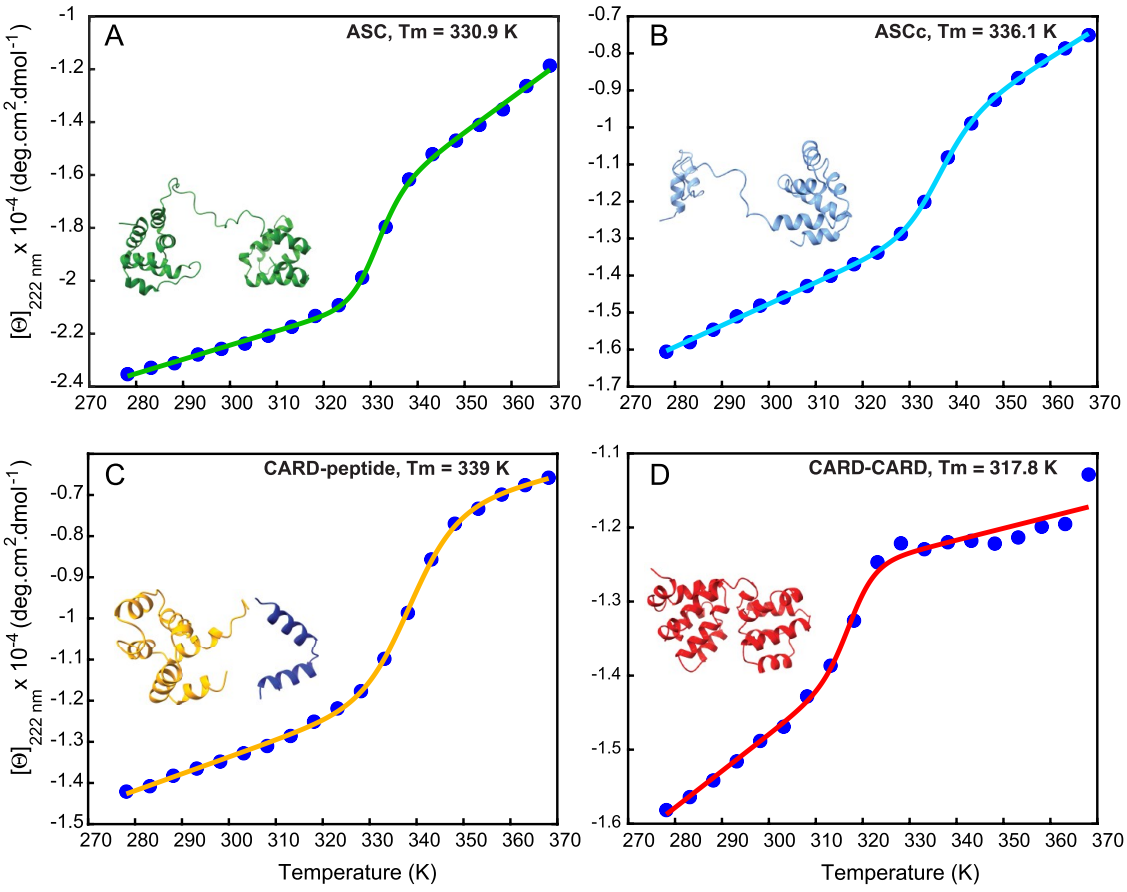

Figure 11. Variations in the stability of ASC-inspired proteins revealed by different melting temperatures. Mean residue ellipticity (Θ) at a wavelength of 222 nm as a function of the temperature (blue circles) of ASC-inspired protein solutions: (A) ASC, (B) ASCc, (C) CARD-peptide, and (D) CARD−CARD. The melting temperature obtained by fitting to a two-state model[36,37] (continuous line) is shown in the corresponding panel. The mean residue ellipticity value at the highest temperature in panel (D) was not included in the fit.

which require specific strategies in recombinant technologies and protein chemistry for their expression and purification. Examples of these strategies include the addition of solubilization tags, the use of mild detergents and denaturants, the elimination of dialysis steps, and working at low protein concentrations.

Our characterization of the viscoelastic behavior of ASC-inspired hydrogels reveals predominantly solid-like mechanical responses as expected for intrinsic physical cross-linkages. However, the designed CARD-peptide hydrogel is stiffer than the natural ASC and ASCc hydrogels and the engineered CARD−CARD. The structural studies by TEM and SEM do not report significant variations between the hydrogels that could explain the different viscoelastic behavior. However, because globular protein domains are the hydrogels' building blocks, we speculate whether their specific structure and stability could cause variations in the mechanical properties. In this regard, our CD results suggest that the CARD-peptide is subjected to more pronounced helical rearrangements upon pH increase because of protein self-association. In addition, the thermal unfolding studies indicate that the CARD-peptide is the most stable protein based on the melting temperature data. These results correlate with the significantly higher values of the storage and loss moduli for CARD-peptide. In contrast, the melting temperature of CARD−CARD is lower than for the other proteins, whereas the G' and G'' values are comparable to ASC and ASCc. Other factors could also play a role in the observed variations of the viscoelastic properties. For instance, the linkers connecting the protein domains are of different lengths (Figure 1), which could affect the rheological response. The linker tethering the PYD and CARD in ASC is composed of 23 amino acids, whereas the linker in CARD−CARD is 3 amino acids long. The CARD-peptide does not have a linker, as this is a heterotypic hydrogel.

As previously reported, the viscoelastic behavior of globular protein hydrogels at the molecular level does not only depend on the cross-linkages but on the load-bearing modules (proteins chains) as well.[1,17,23−25] When globular protein-based hydrogels are subjected to mechanical forces, the cross-linkages are considered the force transducers, whereas the load-bearing modules control the mechanical response.[17] Mechanical forces can unfold globular proteins; thus, the unfolding/folding processes become critical factors controlling the hydrogel viscoelastic response. The cross-linkages in ASC-inspired hydrogels are formed by the entanglement of filaments and fibrils via electrostatic and hydrophobic interactions. However, the load-bearing modules are the actual globular domains and the linkers connecting them. Therefore, upon the exertion of mechanical stress, the proteins of ASC-inspired hydrogels with different domains and linkers could follow several unfolding pathways, resulting in variations in energy dissipation and polymer extension and ultimately leading to discrepant viscoelastic behaviors.

https://doi.org/10.1021/acs.biomac.3c00409
Biomacromolecules 2023, 24, 5563−5577

Further research is needed to investigate the mechanical unfolding of ASC and ASC-inspired proteins as well as to determine the extension of the polypeptide chain upon unfolding. Optical tweezers have been extensively used to determine the mechanical forces required to unfold proteins as well as the overall dimensions of the extended polymer chain.[52] These experiments typically require adding DNA handles to the protein for tethering between two optically trapped micrometer-size beads. Manipulation of the beads via strong infrared lasers allows conducting force−extension experiments on the protein.[53] These studies could shed light on the different viscoelastic responses of the ASC-inspired hydrogels. Understanding the molecular bases responsible for the mechanical properties of these hydrogels will be key to designing potential biotechnological applications.

Importantly, ASC-inspired hydrogels can serve as models to study natural biological hydrogelation processes and to investigate the influence of load-bearing modules (proteins) on the hydrogel mechanical behavior in the absence of artificial cross-linkers. In addition, ASC-inspired hydrogels could have anti-inflammatory applications to capture or retain, via homotypic interactions, inflammatory proteins composed of CARDs and PYDs. Specifically, ASC-inspired hydrogels could be used to capture extracellular inflammasomes that have been reported to amplify the inflammatory response.[54] The pH responsiveness of the ASC-inspired hydrogel could be leveraged to modulate the hydrogel stiffness, specifically for applications that require injectable or sprayable hydrogels. Finally, the hydrogelation capabilities of ASC and its isoforms point to the hypothesis of whether inflammasomes behave as hydrogel-like biomolecular condensates. ASC-inspired hydrogels could be used to investigate this hypothesis.

■ ASSOCIATED CONTENT

Supporting Information

The Supporting Information is available free of charge at https://pubs.acs.org/doi/10.1021/acs.biomac.3c00409.

Amino acid sequence of ASC and ASC-derived protein constructs used for hydrogel formation; hydrogelation process of the CARD-only protein; effect of protein concentration on the flowability of CARD−CARD hydrogels; and pH-responsive behavior of ASC-inspired hydrogels (PDF)

■ AUTHOR INFORMATION

Corresponding Author

Eva de Alba − *Department of Bioengineering, University of California, Merced, Merced, California 95343, United States;* orcid.org/0000-0002-4794-5728; Email: edealbabastarrechea@ucmerced.edu

Authors

Eduardo A. Gaspar-Morales − *Department of Bioengineering and Bioengineering Graduate Program, University of California, Merced, Merced, California 95343, United States*

Anthony Waterston − *Department of Bioengineering and Bioengineering Graduate Program, University of California, Merced, Merced, California 95343, United States;* Present Address: Certified Laboratories, Inc. Turlock, California 95380, United States

Mourad Sadqi − *Department of Bioengineering and NSF CREST Center for Cellular and Biomolecular Machines, University of California, Merced, Merced, California 95343, United States*

Pedro Diaz-Parga − *Department of Bioengineering and Quantitative and Systems Biology Graduate Program, University of California, Merced, Merced, California 95343, United States;* Present Address: Frederick National Laboratory, Frederick, Maryland 21701, United States.

Ariell M. Smith − *Department of Bioengineering, Department of Materials Science and Engineering, and Materials and Biomaterials Science and Engineering Graduate Program, University of California, Merced, Merced, California 95343, United States*

Arvind Gopinath − *Department of Bioengineering and Health Sciences Research Institute, University of California, Merced, Merced, California 95343, United States*

Roberto C. Andresen Eguiluz − *Department of Materials Science and Engineering and Health Sciences Research Institute, University of California, Merced, Merced, California 95343, United States;* orcid.org/0000-0002-5209-4112

Complete contact information is available at: https://pubs.acs.org/10.1021/acs.biomac.3c00409

Notes

The authors declare no competing financial interest.

■ ACKNOWLEDGMENTS

P.D.-P., A.W., and E.d.A. acknowledge the National Institute of Allergy and Infectious Diseases of the National Institutes of Health for financial support under award numbers R15AI146780 and R21AI178831 to E.d.A. and R15AI146780-01S1 to A.W. and E.d.A. P.D.-P., A.W., A.M.S., E.A.G.-M, A.G., R.C.A.E., and E.d.A. acknowledge support from the NSF-CREST Center for Cellular and Biomolecular Machines at the University of California, Merced (NSF-HRD-1547848 and NSF-HRD-2112675) for mass spectrometry data acquisition and analysis. A.M.S. and A.G. acknowledge funding through NSF CBET 2047210. The authors thank UC Merced Imaging facility for access to the TEM and SEM equipment. They are grateful to Dr. Victor Muñoz (University of California, Merced) for access to the CD instrument, Dr. Yue Wang (University of California, Merced) and Dr. Anand Ramasubramanian (San Jose State University) for access to their rheometer instrument. They thank Ayomide J. Adeoye and Zahra Fayaziboroujeni for assistance in pH-reversibility experiments. The content of this publication is solely the responsibility of the authors and does not necessarily represent the official views of the National Institutes of Health or the National Science Foundation.

■ REFERENCES

(1) Li, Y.; Xue, B.; Cao, Y. 100th Anniversary of Macromolecular Science Viewpoint: Synthetic Protein Hydrogels. *ACS Macro Lett.* **2020**, *9* (4), 512−524.

(2) Yang, T.; Wang, L.; Wu, W.-H.; Wei, S.; Zhang, W.-B. Orchestrating Chemical and Physical Cross-Linking in Protein Hydrogels to Regulate Embryonic Stem Cell Growth. *ACS Macro Lett.* **2023**, *12* (2), 269−273.

(3) Huerta-López, C.; Alegre-Cebollada, J. Protein Hydrogels: The Swiss Army Knife for Enhanced Mechanical and Bioactive Properties of Biomaterials. *Nanomaterials* **2021**, *11* (7), 1656.

(4) Ahn, W.; Lee, J.-H.; Kim, S. R.; Lee, J.; Lee, E. J. Designed Protein- and Peptide-Based Hydrogels for Biomedical Sciences. *J. Mater. Chem. B* **2021**, *9* (8), 1919−1940.

(5) Jonker, A. M.; Löwik, D. W. P. M.; van Hest, J. C. M. Peptide- and Protein-Based Hydrogels. *Chem. Mater.* **2012**, *24* (5), 759−773.
(6) *Functional Biopolymers*; Jafar Mazumder, M. A.; Sheardown, H.; Al-Ahmed, A., Eds.; Springer International Publishing: Cham, 2019. DOI: 10.1007/978-3-319-95990-0.
(7) Mizuguchi, Y.; Mashimo, Y.; Mie, M.; Kobatake, E. Temperature-Responsive Multifunctional Protein Hydrogels with Elastin-like Polypeptides for 3-D Angiogenesis. *Biomacromolecules* **2020**, *21* (3), 1126−1135.
(8) Sun, Y.; Li, W.; Wu, X.; Zhang, N.; Zhang, Y.; Ouyang, S.; Song, X.; Fang, X.; Seeram, R.; Xue, W.; He, L.; Wu, W. Functional Self-Assembling Peptide Nanofiber Hydrogels Designed for Nerve Degeneration. *ACS Appl. Mater. Interfaces* **2016**, *8* (3), 2348−2359.
(9) Wagner, C. E.; Krupkin, M.; Smith-Dupont, K. B.; Wu, C. M.; Bustos, N. A.; Witten, J.; Ribbeck, K. Comparison of Physicochemical Properties of Native Mucus and Reconstituted Mucin Gels. *Biomacromolecules* **2023**, *24* (2), 628−639.
(10) Miranda-Nieves, D.; Chaikof, E. L. Collagen and Elastin Biomaterials for the Fabrication of Engineered Living Tissues. *ACS Biomater Sci. Eng.* **2017**, *3* (5), 694−711.
(11) Zhang, Y.; Desai, M. S.; Wnag, T.; Lee, S.-W. Elastin-Based Thermoresponsive Shape-Memory Hydrogels. *Biomacromolecules* **2020**, *21* (3), 1149−1156.
(12) Van Vlierberghe, S.; Dubruel, P.; Schacht, E. Biopolymer-Based Hydrogels As Scaffolds for Tissue Engineering Applications: A Review. *Biomacromolecules* **2011**, *12* (5), 1387−1408.
(13) Banta, S.; Wheeldon, I. R.; Blenner, M. Protein Engineering in the Development of Functional Hydrogels. *Annu. Rev. Biomed. Eng.* **2010**, *12* (1), 167−186.
(14) Hume, J.; Sun, J.; Jacquet, R.; Renfrew, P. D.; Martin, J. A.; Bonneau, R.; Gilchrist, M. L.; Montclare, J. K. Engineered Coiled-Coil Protein Microfibers. *Biomacromolecules* **2014**, *15* (10), 3503−3510.
(15) Petka, W. A.; Harden, J. L.; McGrath, K. P.; Wirtz, D.; Tirrell, D. A. Reversible Hydrogels from Self-Assembling Artificial Proteins. *Science* **1998**, *281* (5375), 389−392.
(16) Haines-Butterick, L.; Rajagopal, K.; Branco, M.; Salick, D.; Rughani, R.; Pilarz, M.; Lamm, M. S.; Pochan, D. J.; Schneider, J. P. Controlling Hydrogelation Kinetics by Peptide Design for Three-Dimensional Encapsulation and Injectable Delivery of Cells. *Proc. Natl. Acad. Sci. U.S.A.* **2007**, *104* (19), 7791−7796.
(17) Wu, J.; Li, P.; Dong, C.; Jiang, H.; Xue, B.; Gao, X.; Qin, M.; Wang, W.; Chen, B.; Cao, Y. Rationally Designed Synthetic Protein Hydrogels with Predictable Mechanical Properties. *Nat. Commun.* **2018**, *9* (1), No. 620.
(18) Lu, H. D.; Charati, M. B.; Kim, I. L.; Burdick, J. A. Injectable Shear-Thinning Hydrogels Engineered with a Self-Assembling Dock-and-Lock Mechanism. *Biomaterials* **2012**, *33* (7), 2145−2153.
(19) Fu, L.; Haage, A.; Kong, N.; Tanentzapf, G.; Li, H. Dynamic Protein Hydrogels with Reversibly Tunable Stiffness Regulate Human Lung Fibroblast Spreading Reversibly. *Chem. Commun.* **2019**, *55* (36), 5235−5238.
(20) Zakeri, B.; Fierer, J. O.; Celik, E.; Chittock, E. C.; Schwarz-Linek, U.; Moy, V. T.; Howarth, M. Peptide Tag Forming a Rapid Covalent Bond to a Protein, through Engineering a Bacterial Adhesin. *Proc. Natl. Acad. Sci. U.S.A.* **2012**, *109* (12), E690−E697.
(21) Guan, D.; Ramirez, M.; Shao, L.; Jacobsen, D.; Barrera, I.; Lutkenhaus, J.; Chen, Z. Two-Component Protein Hydrogels Assembled Using an Engineered Disulfide-Forming Protein−Ligand Pair. *Biomacromolecules* **2013**, *14* (8), 2909−2916.
(22) Wong Po Foo, C. T. S.; Lee, J. S.; Mulyasasmita, W.; Parisi-Amon, A.; Heilshorn, S. C. Two-Component Protein-Engineered Physical Hydrogels for Cell Encapsulation. *Proc. Natl. Acad. Sci. U.S.A.* **2009**, *106* (52), 22067−22072.
(23) Hanson, B. S.; Dougan, L. Network Growth and Structural Characteristics of Globular Protein Hydrogels. *Macromolecules* **2020**, *53* (17), 7335−7345.
(24) Hughes, M. D. G.; Cussons, S.; Mahmoudi, N.; Brockwell, D. J.; Dougan, L. Single Molecule Protein Stabilisation Translates to Macromolecular Mechanics of a Protein Network. *Soft Matter* **2020**, *16* (27), 6389−6399.
(25) Fang, J.; Mehlich, A.; Koga, N.; Huang, J.; Koga, R.; Gao, X.; Hu, C.; Jin, C.; Rief, M.; Kast, J.; Baker, D.; Li, H. Forced Protein Unfolding Leads to Highly Elastic and Tough Protein Hydrogels. *Nat. Commun.* **2013**, *4* (1), No. 2974.
(26) Qian, Z.-G.; Zhou, M.-L.; Song, W.-W.; Xia, X.-X. Dual Thermosensitive Hydrogels Assembled from the Conserved C-Terminal Domain of Spider Dragline Silk. *Biomacromolecules* **2015**, *16* (11), 3704−3711.
(27) Song, W.-W.; Qian, Z.-G.; Liu, H.; Chen, H.-F.; Kaplan, D. L.; Xia, X.-X. On-Demand Regulation of Dual Thermosensitive Protein Hydrogels. *ACS Macro Lett.* **2021**, *10* (4), 395−400.
(28) Arndt, T.; Jaudzems, K.; Shilkova, O.; Francis, J.; Johansson, M.; Laity, P. R.; Sahin, C.; Chatterjee, U.; Kronqvist, N.; Barajas-Ledesma, E.; Kumar, R.; Chen, G.; Strömberg, R.; Abelein, A.; Langton, M.; Landreh, M.; Barth, A.; Holland, C.; Johansson, J.; Rising, A. Spidroin N-Terminal Domain Forms Amyloid-like Fibril Based Hydrogels and Provides a Protein Immobilization Platform. *Nat. Commun.* **2022**, *13* (1), No. 4695.
(29) Park, H. H.; Lo, Y.-C.; Lin, S.-C.; Wang, L.; Yang, J. K.; Wu, H. The Death Domain Superfamily in Intracellular Signaling of Apoptosis and Inflammation. *Annu. Rev. Immunol.* **2007**, *25* (1), 561−586.
(30) de Alba, E. Structure, Interactions and Self-Assembly of ASC-Dependent Inflammasomes. *Arch. Biochem. Biophys.* **2019**, *670*, 15−31.
(31) de Alba, E. Structure and Interdomain Dynamics of Apoptosis-Associated Speck-like Protein Containing a CARD (ASC). *J. Biol. Chem.* **2009**, *284* (47), 32932−32941.
(32) Diaz-Parga, P.; de Alba, E. Protein Interactions of the Inflammasome Adapter ASC by Solution NMR. *Methods Enzymol.* **2019**, *625*, 223−252.
(33) Bryan, N. B.; Dorfleutner, A.; Kramer, S. J.; Yun, C.; Rojanasakul, Y.; Stehlik, C. Differential Splicing of the Apoptosis-Associated Speck like Protein Containing a Caspase Recruitment Domain (ASC) Regulates Inflammasomes. *J. Inflammation* **2010**, *7* (1), No. 23.
(34) Expasy. https://www.expasy.org.
(35) Shy, A. N.; Wang, H.; Feng, Z.; Xu, B. Heterotypic Supramolecular Hydrogels Formed by Noncovalent Interactions in Inflammasomes. *Molecules* **2021**, *26* (1), 77.
(36) Naganathan, A. N.; Perez-Jimenez, R.; Sanchez-Ruiz, J. M.; Muñoz, V. Robustness of Downhill Folding: Guidelines for the Analysis of Equilibrium Folding Experiments on Small Proteins. *Biochemistry* **2005**, *44* (20), 7435−7449.
(37) Sborgi, L.; Verma, A.; Piana, S.; Lindorff-Larsen, K.; Cerminara, M.; Santiveri, C. M.; Shaw, D. E.; de Alba, E.; Muñoz, V. Interaction Networks in Protein Folding via Atomic-Resolution Experiments and Long-Time-Scale Molecular Dynamics Simulations. *J. Am. Chem. Soc.* **2015**, *137* (20), 6506−6516.
(38) Nambayan, R. J. T.; Sandin, S. I.; Quint, D. A.; Satyadi, D. M.; de Alba, E. The Inflammasome Adapter ASC Assembles into Filaments with Integral Participation of Its Two Death Domains, PYD and CARD. *J. Biol. Chem.* **2019**, *294* (2), 439−452.
(39) Oroz, J.; Barrera-Vilarmau, S.; Alfonso, C.; Rivas, G.; de Alba, E. ASC Pyrin Domain Self-Associates and Binds NLRP3 Protein Using Equivalent Binding Interfaces*. *J. Biol. Chem.* **2016**, *291* (37), 19487−19501.
(40) Wang, H.; Feng, Z.; Lu, A.; Jiang, Y.; Wu, H.; Xu, B. Instant Hydrogelation Inspired by Inflammasomes. *Angew. Chem., Int. Ed.* **2017**, *56* (26), 7579−7583.
(41) Yang, J.; Zhang, Y. I-TASSER Server: New Development for Protein Structure and Function Predictions. *Nucleic Acids Res.* **2015**, *43* (W1), W174−W181.
(42) Pettersen, E. F.; Goddard, T. D.; Huang, C. C.; Meng, E. C.; Couch, G. S.; Croll, T. I.; Morris, J. H.; Ferrin, T. E. UCSF ChimeraX: Structure Visualization for Researchers, Educators, and Developers. *Protein Sci.* **2021**, *30* (1), 70−82.

(43) Sharma, M.; de Alba, E. Structure, Activation and Regulation of NLRP3 and AIM2 Inflammasomes. *Int. J. Mol. Sci.* **2021**, *22* (2), 872.
(44) Zhou, W.; Kaneko, N.; Nakagita, T.; Takeda, H.; Masumoto, J. A Comprehensive Interaction Study Provides a Potential Domain Interaction Network of Human Death Domain Superfamily Proteins. *Cell Death Differ.* **2021**, *28* (11), 2991−3008.
(45) Diaz-Parga, P.; de Alba, E. Inflammasome Regulation by Adaptor Isoforms, ASC and ASCb, via Differential Self-Assembly. *J. Biol. Chem.* **2022**, *298* (3), No. 101566.
(46) Diaz-Parga, P.; Gould, A.; de Alba, E. Natural and Engineered Inflammasome Adapter Proteins Reveal Optimum Linker Length for Self-Assembly. *J. Biol. Chem.* **2022**, *298* (11), No. 102501.
(47) Pal, A.; Neo, K.; Rajamani, L.; Ferrer, F. J.; Lane, D. P.; Verma, C. S.; Mortellaro, A. Inhibition of NLRP3 Inflammasome Activation by Cell-Permeable Stapled Peptides. *Sci. Rep.* **2019**, *9* (1), No. 4913.
(48) Zhou, N. E.; Kay, C. M.; Hodges, R. S. Synthetic Model Proteins: The Relative Contribution of Leucine Residues at the Nonequivalent Positions of the 3−4 Hydrophobic Repeat to the Stability of the Two-Stranded α-Helical Coiled-Coil. *Biochemistry* **1992**, *31* (25), 5739−5746.
(49) Potekhin, S. A.; Melnik, T. N.; Popov, V.; Lanina, N. F.; Vazina, A. A.; Rigler, P.; Verdini, A. S.; Corradin, G.; Kajava, A. V. De Novo Design of Fibrils Made of Short α-Helical Coiled Coil Peptides. *Chem. Biol.* **2001**, *8* (11), 1025−1032.
(50) Li, Y.; Fu, T.-M.; Lu, A.; Witt, K.; Ruan, J.; Shen, C.; Wu, H. Cryo-EM Structures of ASC and NLRC4 CARD Filaments Reveal a Unified Mechanism of Nucleation and Activation of Caspase-1. *Proc. Natl. Acad. Sci. U.S.A.* **2018**, *115* (43), 10845−10852.
(51) Lu, A.; Magupalli, V. G.; Ruan, J.; Yin, Q.; Atianand, M. K.; Vos, M. R.; Schröder, G. F.; Fitzgerald, K. A.; Wu, H.; Egelman, E. H. Unified Polymerization Mechanism for the Assembly of ASC-Dependent Inflammasomes. *Cell* **2014**, *156* (6), 1193−1206.
(52) Bustamante, C. J.; Chemla, Y. R.; Liu, S.; Wang, M. D. Optical Tweezers in Single-Molecule Biophysics. *Nat. Rev. Methods Primers* **2021**, *1* (1), No. 25.
(53) Bustamante, C.; Alexander, L.; Maciuba, K.; Kaiser, C. M. Single-Molecule Studies of Protein Folding with Optical Tweezers. *Annu. Rev. Biochem.* **2020**, *89* (1), 443−470.
(54) Baroja-Mazo, A.; Martín-Sánchez, F.; Gomez, A. I.; Martínez, C. M.; Amores-Iniesta, J.; Compan, V.; Barberà-Cremades, M.; Yagüe, J.; Ruiz-Ortiz, E.; Antón, J.; Buján, S.; Couillin, I.; Brough, D.; Arostegui, J. I.; Pelegrín, P. The NLRP3 Inflammasome Is Released as a Particulate Danger Signal That Amplifies the Inflammatory Response. *Nat. Immunol.* **2014**, *15* (8), 738−748.

NOTE ADDED AFTER ASAP PUBLICATION

This paper was originally published ASAP on November 6, 2023, with an error in the *y*-axis of Figure 3. The corrected version was reposted on November 20, 2023.

https://doi.org/10.1021/acs.biomac.3c00409
Biomacromolecules 2023, 24, 5563−5577